Origin of the anomalous contributions to the ac magnetic susceptibility of rare-earth–iron intermetallic compounds

C. Piquer and J. Bartolomé
Departamento de Física de la Materia Condensada, Instituto de Ciencia de Materiales de Aragón, Consejo Superior de Investigaciones Científicas, Universidad de Zaragoza, 50009 Zaragoza, Spain

C. de Francisco and J. M. Muñoz
Departamento de Electricidad y Electrónica, Universidad de Valladolid, 47071 Valladolid, Spain
(Received 11 December 2008; revised manuscript received 20 March 2009; published 26 May 2009)

A systematic ac magnetic susceptibility, $\chi_{ac}(T)$, study has been performed on several $R_2Fe_{14}BH_x$ (R=rare earth) compounds in order to determine the origin of the anomalous behavior of $\chi_{ac}(T)$ not related to spin reorientation transitions—the so-called non-SRT anomalies. All the measurements have been performed on magnetically oriented samples to identify the anomalies due to domain-wall displacements. Different types of non-SRT anomalies have been found. It has been found that the anomalous behavior is mainly due to the existence of mobile defects coupled to the domain walls, which existence has been confirmed by performing magnetic aftereffect measurements. However, this mechanism alone cannot explain the whole phenomenology and other influences on $\chi_{ac}(T)$ have to be taken into account to correctly describe the non-SRT anomalies. Specifically, three situations are possible when analyzing the anomalous behavior of $\chi_{ac}(T)$: (1) compounds with no magnetic R anisotropy, in which the non-SRT anomalies are due to the existence of one or more mobile defects coupled to the domain walls, (2) compounds in which a large magnetic R anisotropy can influence the domain-wall mobility at very low temperatures, and (3) compounds in which a large magnetic R anisotropy and the existence of SRTs can influence the response of the domain walls coupled to mobile defects. Different fitting models have been proposed for each case.

DOI: 10.1103/PhysRevB.79.174430 PACS number(s): 75.30.Gw, 75.50.Bb, 75.50.Ww, 75.60.Ch

I. INTRODUCTION

The measurement of the ac initial magnetic-susceptibility temperature dependence, $\chi_{ac}(T)$, is a common procedure to study the magnetic properties of R-T (R=rare earth, T=transition metal) intermetallic compounds.[1] It has been widely used to detect magnetic phase transitions, such as spin reorientations transitions (SRTs).[1,2] In the $R_2Fe_{14}B$ compounds, a rounded maximum is observed in $\chi_{ac}(T)$ when a second-order SRT takes place (R=Nd and Ho), whereas a cusplike anomaly is detected in the compounds that present a first-order SRT (R=Er, Tm).[2] However, due to the high sensitivity of the $\chi_{ac}(T)$ technique, it is possible that other mechanisms, of extrinsic origin, may induce anomalies of similar shape in $\chi_{ac}(T)$, the so-called non-SRT anomalies, which have been frequently reported for different R-Fe compounds.[3–9]

Several interpretations have been proposed to explain these non-SRT anomalies (see Ref. 5 for a review), however, most of these interpretations can be ruled out after the work of García *et al.*[5] These authors have shown that in $R_2Fe_{14}BH_x$ (R=Nd and Ho), the non-SRT anomalies display thermal hysteresis, can be induced or enhanced by thermal annealing, are enhanced when the measurements are performed with the applied field parallel to the easy magnetization direction (EMD), and are reduced under application of an external field.[5] Moreover, the non-SRT anomalies can be correlated with the anomalous behavior observed in magnetic aftereffect (MAE) measurements.[5] The same correlation between $\chi_{ac}(T)$ and MAE anomalies is observed for $Sm_2Fe_{17}N_x$ compounds.[4] In both cases the MAE anomalies are originated by thermally activated jumps of iron vacancies or interstitial atoms.[4,5] These experimental findings indicate that[5] (i) the non-SRT anomalies are related to anomalous contributions coming from the domain walls (DWs) and (ii) they depend on the microstructure of the samples, that is, on the presence of impurities or defects.

A characteristic feature of the $\chi_{ac}(T)$ non-SRT anomalies is that they are usually accompanied by another type of anomalous behavior at relatively high temperatures; namely, a sharp increase in the in-phase component, $\chi'_{ac}(T)$, accompanied by a peak in the out-of-phase component, $\chi''_{ac}(T)$.[3–9] This is the case of the $R_2Fe_{14}BH_x$ (R=Nd and Ho) compounds, in which the whole $\chi_{ac}(T)$ anomalous behavior has been described as originated by the presence of mobile defects coupled to the DWs.[5] According to this description, the coupling between defects and DWs produces (1) the appearance of a drop in $\chi'_{ac}(T)$ accompanied by a peak in $\chi''_{ac}(T)$ at relatively low T and (2) a sharp increase in $\chi'_{ac}(T)$ accompanied by a peak in at relative high T.[5]

This model has also been successfully applied in the analysis of $\chi_{ac}(T)$ in different R_2Fe_{17} compounds.[7,8] However, some differences exist regarding the shape of the non-SRT anomalies of the $R_2Fe_{14}BH_x$ and R_2Fe_{17} compounds. In $R_2Fe_{14}BH_x$ (R=Nd and Ho), $\chi'_{ac}(T)$ is nearly zero at low temperatures and the non-SRT anomaly consists of a small peak at $T\sim 100-150$ K (see, for instance, Figs. 18 and 19 of Ref. 5). In $Sm_2Fe_{17}N_x$, $\chi'_{ac}(T)$ is relatively high at low T and a clear drop appears at $T\sim 100-150$ K (see, for instance, Fig. 1 of Ref. 4 or Fig. 20 of Ref. 5).

The R_2Fe_{17} $\chi_{ac}(T)$ non-SRT anomalies have also been described in terms of the influence of the R magnetic crystal-

line anisotropy (MCA) in the DW movements.[6] According to Kou *et al.*,[6] the DWs are extremely narrow at low T; hence, they posses no mobility and $\chi'_{ac}(T) \sim 0$. When the temperature is raised, the MCA diminishes and the DWs become broader. According to the authors, this broadening of the DWs can result in a sharp increase of $\chi'_{ac}(T)$. The $\chi'_{ac}(T)$ low T peak is then interpreted by assuming that at higher temperatures, the DWs are so broad that they become pinned by the surface, causing a drastic reduction in the DWs mobility. However, this argument does not explain either the nonvanishing $\chi''_{ac}(T)$ accompanying the increase in $\chi'_{ac}(T)$ or the cases in which there is another sharp increase in $\chi'_{ac}(T)$ at higher temperatures accompanied by a peak in $\chi''_{ac}(T)$.

In some cases, such as the $R_2Fe_{14}BH_x$ (R=Gd, Pr, and Dy) compounds, the non-SRT anomalies have been interpreted as hydrogen-induced spin reorientation transitions (HISRTs).[10,11] This kind of misinterpretations can be avoided by measuring $\chi_{ac}(T)$ on magnetically oriented samples and by performing some complementary measurements such as magnetization versus temperature or versus field.[9,12] Following this procedure, it was shown that all the $R_2Fe_{14}BH_x$ (R=Gd, Pr, and Dy) compounds except $Gd_2Fe_{14}B$ display non-SRT anomalies, which are due to anomalous contributions coming from the DWs displacements.[9,12] However, the $\chi_{ac}(T)$ anomalous behavior observed in these compounds is rather different from that observed in the R=Nd and Ho series.[5,9] This result indicates that the non-SRT anomaly's phenomenology is more complex than that expected from the study of the R=Nd and Ho series.

The main objective of this work is to provide a better understanding of the $\chi_{ac}(T)$ anomalous behavior in $R_2Fe_{14}BH_x$. In this paper it is shown that, although this anomalous behavior is essentially due to the existence of mobile defects coupled to the DWs, it is necessary to take into account additional effects such as the existence of different kinds of mobile defects coupled to the DWs and the influence of the MCA.

The paper is organized as follows. The experimental details and methods are given in Secs. II and III, the description of the anomalous behavior of $\chi_{ac}(T)$ in $R_2Fe_{14}BH_x$ (R=Gd, Y, Pr, Dy, and Tb) is detailed in Sec. IV, the analysis of this behavior is presented in Sec. V, and, finally, the main conclusions are reported in Sec. VI.

II. EXPERIMENTAL DETAILS

The following samples have been studied: $Gd_2Fe_{14}BH_x$, with x=0, 1, 2, 3, and 4, $Y_2Fe_{14}BH_x$, with x=1, 2.5, and 3.5, $Pr_2Fe_{14}BH_x$, with x=0, 1, 2, 3, and 5.5, $Dy_2Fe_{14}BH_x$, with x=0, 1, 2, and 4, and $Tb_2Fe_{14}BH_x$, with x=1, 2, 2.5, and 3. The details of sample preparation are described in Ref. 12.

Zero-field-cooled $\chi_{ac}(T)$ measurements have been performed in all samples. For $Gd_2Fe_{14}BH_x$, $Pr_2Fe_{14}BH_x$, and $Dy_2Fe_{14}BH_x$, the in-phase, $\chi'_{ac}(T)$, and the out of phase $\chi''_{ac}(T)$ components of the complex ac susceptibility have been measured in a commercial Quantum Design superconducting quantum interference device (SQUID) magnetometer covering a temperature region from 5 K to room temperature, with an exciting field of 5 Oe, and frequencies ranging from 0.90 to 90 Hz. For the $Y_2Fe_{14}BH_x$ and $Tb_2Fe_{14}BH_x$ compounds, $\chi'_{ac}(T)$ and $\chi''_{ac}(T)$ have been measured with a mutual inductance susceptometer covering a temperature region from 5 to 350 K, with an exciting field of 5 Oe, and a frequency of 90 Hz.

In all cases, the $\chi_{ac}(T)$ measurements have been performed on magnetically oriented powders, prepared by embedding the powders into epoxy resin and exposing the mixture to a 5000 Oe field until the epoxy hardened. The nonaxial compound was oriented using a rotating device.[13] $\chi_{\parallel}(T)$ and $\chi_{\perp}(T)$ denote the measurements performed in the parallel and in the perpendicular directions, respectively, with respect to the alignment axis of the epoxy-bonded samples, i.e., with respect to their EMD at room temperature. Consequently, for the compounds displaying a [001] EMD at RT, $\chi_{\parallel}(T)$ and $\chi_{\perp}(T)$ are the ac magnetic susceptibilities measured with the applied field parallel and perpendicular, respectively, to the crystallographic c axis. MAE measurements have been carried out by recording the variation of the initial permeability $\mu=\mu_0(1+\chi)$ as a function of time after demagnetization of the sample with an external ac field.[14]

III. EXPERIMENTAL METHODS

A. ac magnetic-susceptibility measurements

Hard magnets with uniaxial magnetic anisotropy contain 180° domains with their DWs parallel to the magnetic axis.[15,16] In such a case, at low exciting frequency, $\chi_{ac}(T)$ is due to reversible rotation of the magnetic moments within each domain, $\chi_{RR}(T)$, and to DW displacements, $\chi_{DW}(T)$.[3,6,17,18] In the uniaxial magnetic phase, $\chi_{DW}(T)$ is significant only when the exciting field is applied parallel to the DWs. In contrast, it should be zero when the exciting field is applied perpendicular to the DWs because a small perpendicular exciting field does not move the domain walls. Consequently, when analyzing the susceptibility measured on magnetically oriented samples, $\chi_{\parallel}(T)$ and $\chi_{\perp}(T)$, three situations are possible:

(1) Compounds having an [001] EMD in the whole studied thermal range ($Gd_2Fe_{14}BH_x$, $Y_2Fe_{14}BH_x$, $Dy_2Fe_{14}B$, and $Pr_2Fe_{14}BH_x$, with $x<3$).[12] In this case, the $\chi_{DW}(T)$ contribution is zero in $\chi_{\perp}(T)$ and only contributes to $\chi_{\parallel}(T)$. Consequently, any anomalous behavior of $\chi_{\parallel}(T)$ not detected in $\chi_{\perp}(T)$ at the same temperatures is due to DW displacements.

(2) Compounds with an [001] EMD at RT and having a SRT at $T=T_s<$RT ($Dy_2Fe_{14}BH_x$, with $x>1$).[12] At $T>T_s$ the situation is identical to that described in (1); however, when the SRT takes place, the change in the EMD can produce anomalous contributions to $\chi_{\parallel}(T)$ coming from the rotations of the magnetic moments. Moreover, at $T \leq T_s$, when the EMD is no longer along the c axis, the magnetic structure is different than that of 180° domains described above.

(3) Compounds not magnetically axial at RT ($Pr_2Fe_{14}BH_{5.5}$).[12] In such a case, the system does not possess the 180° DW magnetic structure described above and it is not possible to identify the anomalous contributions to $\chi_{ac}(T)$ or to $\chi_{\parallel}(T)$, which are exclusively due to DW displacements.

This procedure has been applied in the study of the $R_2Fe_{14}BH_x$ (R=Gd, Pr, and Dy) to discern whether an

anomaly in $\chi_{ac}(T)$ is due to a SRT.[12] In Sec. IV, it shall be applied to identify whether an anomaly in $\chi_{ac}(T)$, or $\chi_{\parallel}(T)$, is due to DW displacements.

B. Magnetic aftereffect measurements

The presence of mobile defects coupled to the domain walls may give rise to anomalous contributions to $\chi_{ac}(T)$ or to $\chi_{\parallel}(T)$.[4,5,19] The presence of such kind of defects can be evidenced by using the MAE technique, which provides detailed information on intrinsic defects or impurity atoms.[20]

In a general case, the existence of mobile defects coupled to DWs implies the existence of an attractive potential, Φ, describing the interaction between DWs and defects, which act as pinning centers.[5,19,20] When the total DWs-defects system is driven out of equilibrium (by applying a demagnetization procedure, for instance), both DWs and defects are at off-equilibrium positions. As time elapses, the system evolves toward the equilibrium state via thermal-activated process of defects moving toward their minimum-energy positions. Consequently, the evolution of the total system toward the equilibrium is determined by the relaxation time of the defects, τ_d. It is usually assumed that τ_d depends on the temperature following an Arrhenius law, $\tau_d = \tau_0 \exp(Q/k_B T)$, where Q is the activation energy and k_B the Boltzman constant. This relaxation process can be explained as a deepening of the potential wells at which lay the DWs. This deepening is due to a time-dependent component, Φ_t, of the total potential acting on the DWs, $\Phi_{tot} = \Phi_0 + \Phi_t$, where Φ_0 results from the interaction of the domain walls with all defects which are immobile in the observed temperature range. This deepening of the potential well produces a reduction of the domain-wall mobility and, consequently, a decrease of the initial susceptibility.[20] This phenomenon, which results from the stabilization of the DWs in the sample, takes place within a particular temperature range for a given material and is usually referred to as a disaccommodation of the initial susceptibility.

The decrease of the initial susceptibility after the demagnetizing process, which is measured at a given temperature, is known as isothermal relaxation, which is strongly dependent on the temperature. In order to isolate the temperature dependence of a MAE, it is more appropriate to study the so-called isochronal relaxation curves. These curves are constructed by calculating the change of the initial susceptibility, $\Delta\chi$, at temperature T, between two measuring times t_1 and t_2 ($t_2 > t_1$), following the demagnetization of the sample at $t = 0$, $\Delta\chi(t_1, t_2) = \chi(t_1, T) - \chi(t_2, T)$. Repeating this procedure for different temperatures, the isochronal curves $\Delta\chi(t_1, t_2, T)$ for a given t_1 and t_2 are obtained.[20] If a thermally activated relaxation occurs within the thermal range investigated, the resulting isochronal curves exhibit a maximum as that shown in Figs. 1 and 2. Such a maximum can be explained as follows: at very low T, the mobility of the defects is very small; consequently, the relaxation process occurs so slowly that in the time interval $(t_2\text{-}t_1)$ almost no relaxation takes place. The opposite situation takes place at relative high temperatures, when the defects posses a very high mobility. In such a case, the relaxation proceeds so quickly that thermal equilibrium is reached before t_1. Only at intermediate temperatures, when the time interval $(t_2\text{-}t_1)$ is of the same order as the defects relaxation time, there is a nonnegligible contribution to $\Delta\chi(t_1, t_2, T)$.

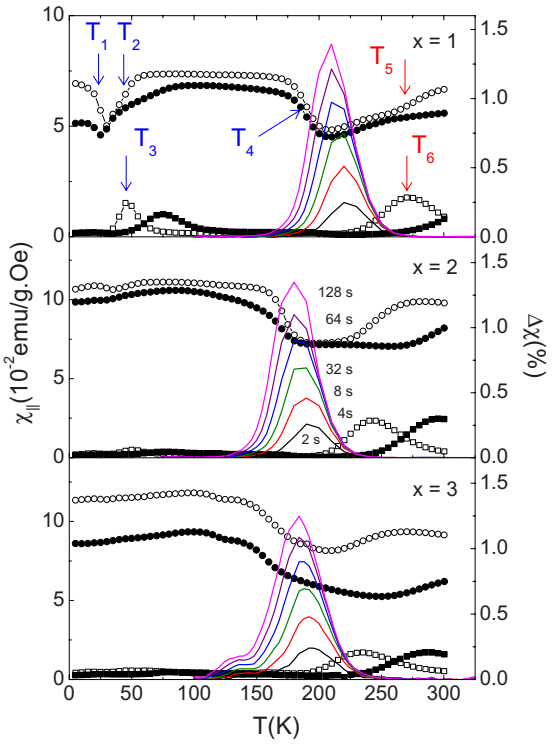

FIG. 1. (Color online) Left scale: In-phase, $\chi'_{\parallel}(T)$ (circles), and out-of-phase, $\chi''_{\parallel}(T)$ (squares), magnetic susceptibilities vs temperature of epoxy-bonded $Gd_2Fe_{14}BH_x$ ($x=1$, 2, and 3) measured along the c axis at $f=0.9$ (open symbols) and 90 Hz (dark symbols). In all cases $\chi''_{\parallel}(T)$ has been multiplied by a factor 2. Right scale: isochronal relaxation curves performed on the same epoxy-oriented $Gd_2Fe_{14}BH_x$ powders measured along the c axis for $t_1 \approx 0$ and $t_2 = 2$ (black), 4 (red), 8 (green), 32 (blue), 64 (purple), and 128 s (pink).

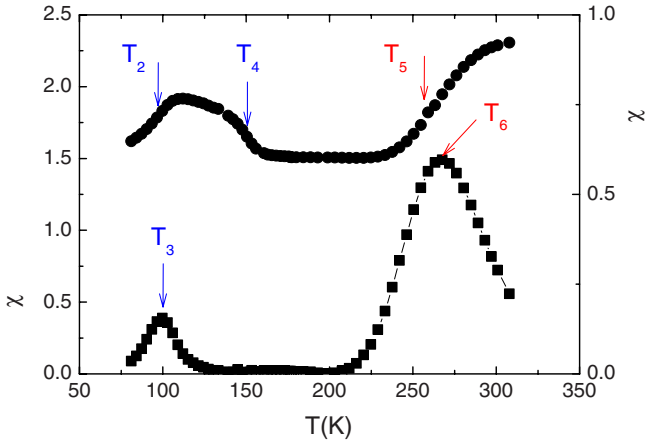

FIG. 2. (Color online) In-phase, $\chi'_{\parallel}(T)$ (dark circles), and out-of-phase, $\chi''_{\parallel}(T)$ (dark squares), magnetic susceptibilities vs temperature of epoxy-bonded $Y_2Fe_{14}BH_{2.5}$ measured along the c axis at $f=90$ Hz.

Usually, there is a distribution of different relaxation times, but in general it is assumed that they may be averaged, yielding the following expression for the isochronal curves:

$$\Delta\chi(t_1,t_2,T) = \sum_i \Delta\chi_i\{\exp[-t_1/\tau_i(T)] - \exp[-t_2/\tau_i(T)]\}. \quad (1)$$

Fitting the MAE curves to this expression for different values of t_1 and t_2 it is possible to determine the parameters τ_{0i} and Q_i,[21] which characterize the relaxation process due to the presence of mobile defects coupled to the DWs.

IV. EXPERIMENTAL RESULTS

A. ac magnetic-susceptibility measurements

1. $Gd_2Fe_{14}BH_x$ and $Y_2Fe_{14}BH_x$

In pure $Gd_2Fe_{14}B$ there is no anomalous behavior either in $\chi_\parallel(T)$ or in $\chi_\perp(T)$.[9,12] Moreover, no anomalous behavior is detected in $\chi_\perp(T)$ of the hydrogenated compounds.[12] Consequently, all the anomalous behaviors found in $\chi_\parallel(T)$, displayed in Fig. 1, are due to anomalous contributions coming from the DWs displacements. In this figure the MAE experiments performed on the same samples are also displayed.

This peculiar behavior of $\chi_\parallel(T)$ is not exclusive of the Gd compounds, similar $\chi_\parallel(T)$ curves are also found in $Y_2Fe_{14}BH_x$, which are displayed in Fig. 2. Although the measurements on the $Y_2Fe_{14}BH_x$ samples are taken in the temperature range of 80–350 K, some common features are clearly observed: relative high values of $\chi_\parallel(T)$ at low temperatures and the same type of low-temperature (LT) anomalies described by T_2 and T_3 in $Gd_2Fe_{14}BH$.

2. $Pr_2Fe_{14}BH_x$

All $Pr_2Fe_{14}BH_x$ with $x<5.5$ are magnetically axial in the whole measured thermal range and none of them displays anomalous behavior in $\chi_\perp(T)$.[12] Consequently, all the anomalous behaviors found in $\chi_\parallel(T)$ (see Fig. 3) are due to anomalous contributions coming from the DW displacements. By analogy with the Gd series, the same notation for the $\chi_\parallel(T)$ anomalies is used. In Fig. 3 the MAE experiments performed on the same samples are displayed.

$Pr_2Fe_{14}B$ displays a clear peak in $\chi'_\parallel(T)$ around 150 K, accompanied by another peak in $\chi''_\parallel(T)$ at T_3. The LT tail of the $\chi'_\parallel(T)$ peak depends on the frequency of the applied alternating field (specially for $x>0$), whereas the high-temperature (HT) tail does not. For $x=2$, around 220 K, a new increase appears in $\chi'_\parallel(T)$ at T_5, accompanied by a peak in $\chi''_\parallel(T)$ at T_6. The onset of such behavior is also observable for $x=1$ at 290 K. These increases, and the corresponding peaks in $\chi''_\parallel(T)$, shift to higher temperature for increasing frequency and to lower temperature for increasing hydrogen content. The behavior of $\chi'_\parallel(T)$ at $T>200$ K is in agreement with the existence of mobile defects coupled to the DWs.[5] In such a case, the HT tail of the $\chi'_\parallel(T)$ peak (which is frequency independent) can be seen as an independent drop of $\chi'_\parallel(T)$, similar to that observed in $Gd_2Fe_{14}BH_x$.

The $\chi_\parallel(T)$ anomalous behavior of $Pr_2Fe_{14}BH_x$ resembles that of $Nd_2Fe_{14}BH_x$ and $Ho_2Fe_{14}BH_x$. That is, $\chi'_\parallel(T)$ is almost zero at very low temperatures and a peak is observed in both $\chi'_\parallel(T)$ and $\chi''_\parallel(T)$ at intermediate temperatures ($\sim$150 K). However, in $Pr_2Fe_{14}BH_x$ the $\chi'_\parallel(T)$ peak is much larger than those observed in the R=Nd and Ho series and cannot be described as a simple drop in $\chi'_\parallel(T)$. Moreover, as in $Gd_2Fe_{14}BH_x$, there is no peak in $\chi''_\parallel(T)$ accompanying the drop of $\chi'_\parallel(T)$ at $T_4\sim200$ K, whereas a clear peak in $\chi''_\parallel(T)$ appears accompanying the LT tail of the peak in $\chi'_\parallel(T)$.

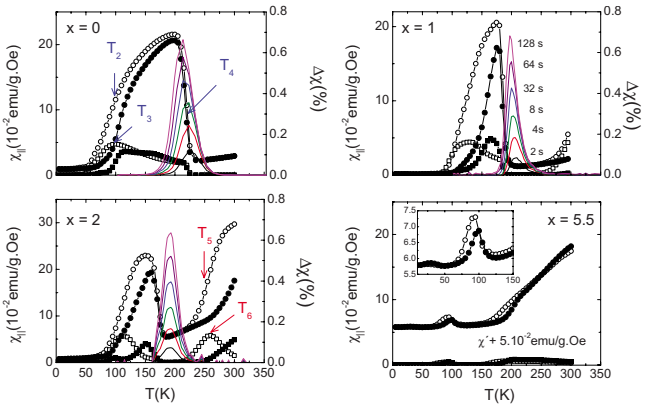

FIG. 3. (Color online) Left scale: In-phase, $\chi'_\parallel(T)$ (circles), and out-of-phase, $\chi''_\parallel(T)$ (squares), magnetic susceptibilities vs temperature of epoxy-bonded $Pr_2Fe_{14}BH_x$ (x=0, 1, 2, and 5.5) measured along the c axis at f=0.9 (open symbols) and 90 Hz (dark symbols). For the sake of clarity, $\chi'_\parallel(T)$ of the $Pr_2Fe_{14}BH_{5.5}$ compound has been vertically shifted by 5.10^{-2} emu/g Oe. Right scale: isochronal relaxation curves performed on the same epoxy-oriented $Pr_2Fe_{14}BH_x$ powders measured along the c axis for $t_1\approx0$, and t_2 =2 (black), 4 (red), 8 (green), 32 (blue), 64 (purple), and 128 s (pink).

The $Pr_2Fe_{14}BH_{5.5}$ compound is not magnetically axial in the measured temperature range. Hence, the anomalies detected in $\chi_\parallel(T)$ cannot be exclusively attributed to DW displacements. Indeed, the $\chi_\parallel(T)$ behavior of this compound is different from that observed in the $x<5.5$ compounds; similar anomalies are observed, but they are less defined and display little frequency dependence.

A final comment is devoted to the anomaly detected in pure $Pr_2Fe_{14}B$. In this compound the $\chi'_\parallel(T)$ peak is broader than those observed in the hydrogenated compounds, moreover, it is accompanied by a nonzero $\chi''_\parallel(T)$ in the range of 50–225 K. A similar change in the shape of the LT $\chi'_\parallel(T)$ peak has also been reported for R_2Fe_{17} and $R_2Fe_{17}H_x$ compounds.[7]

3. $Dy_2Fe_{14}BH_x$ and $Tb_2Fe_{14}BH_x$

The $\chi_\parallel(T)$ curves of $Dy_2Fe_{14}BH_x$ are shown in Fig. 4 together with the MAE measurements and the $\chi_\perp(T)$ curves showing the HISRT that takes place in the $Dy_2Fe_{14}BH_x$ compounds for $x>1$. By analogy with the other series, the same notation for the anomalies is used.

$Dy_2Fe_{14}B$ does not display any anomalous behavior in $\chi_\perp(T)$ (see Fig. 4). Hence, the anomalous behavior of $\chi_\parallel(T)$ is due to the DWs contribution. In $Dy_2Fe_{14}BH$, both $\chi'_\parallel(T)$ and $\chi''_\parallel(T)$ are nearly zero up to 200 K (note that in Fig. 4 $\chi'_\parallel(T)$ has been vertically shifted by $0.5.10^{-2}$ emu/g Oe) and

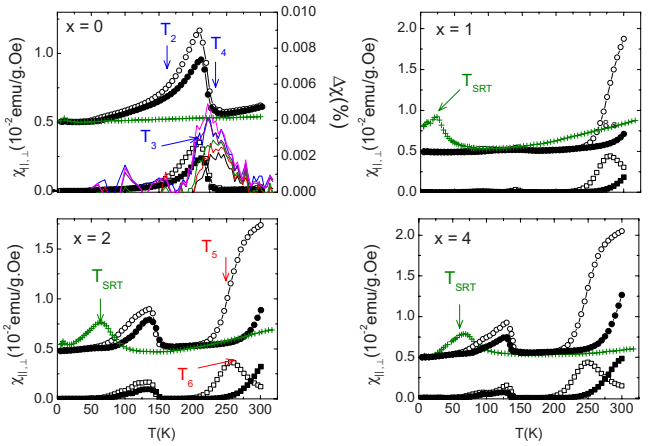

FIG. 4. (Color online) Left scale: In-phase, $\chi'_{\parallel}(T)$ (circles), and out-of-phase, $\chi''_{\parallel}(T)$ (squares), magnetic susceptibilities vs temperature of epoxy-bonded $Dy_2Fe_{14}BH_x$ (x=0, 1, 2, and 4) measured along the c axis at f=0.9 (open symbols) and 90 Hz (dark symbols). In the same scale the in-phase $\chi'_{\perp}(T)$ (crosses, green) magnetic susceptibility measured perpendicular to the c axis at f=90 Hz is also displayed. For the sake of clarity, $\chi'_{\parallel}(T)$ and $\chi'_{\perp}(T)$ have been vertically shifted by $0.5.10^{-2}$emu/g Oe and $\chi'_{\perp}(T)$ of the $Dy_2Fe_{14}BH$ compound has been multiplied by 3. Right scale: isochronal relaxation curves performed on the same epoxy-oriented $Dy_2Fe_{14}BH_x$ powders measured along the c axis for $t_1 \approx 0$ and t_2 =2 (black), 4 (red), 8 (green), 32 (blue), 64 (purple), and 128 s (pink).

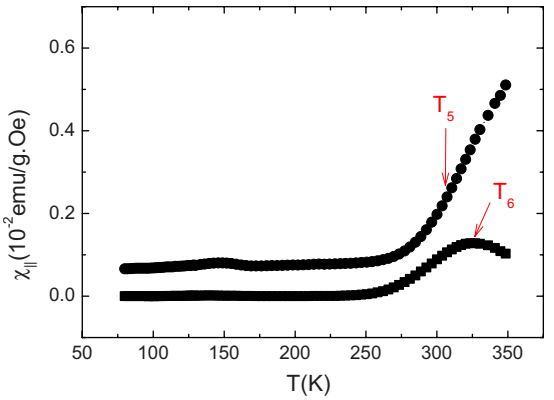

FIG. 5. (Color online) In-phase, $\chi'_{\parallel}(T)$ (dark circles), and out-of-phase, $\chi''_{\parallel}(T)$ (dark squares), magnetic susceptibilities vs temperature of epoxy-bonded $Tb_2Fe_{14}BH_2$ measured along the c axis at f=90 Hz.

only the usual steplike increase in $\chi'_{\parallel}(T)$ at T_5 accompanied by a peak in $\chi''_{\parallel}(T)$ at T_6 is observed. This behavior also appears in the $x>1$ compounds and shifts to lower temperatures for increasing the hydrogen content. For $x>1$ a small peak appears at $T \sim 125-150$ K.

The anomalous behavior of $\chi_{\parallel}(T)$ in $Dy_2Fe_{14}BH_x$ compounds is nearly identical to that observed in $Nd_2Fe_{14}BH_x$ and $Ho_2Fe_{14}BH_x$ (see, for instance, Figs. 18 and 19 of Ref. 5). In contrast, significant differences are observed when comparing to the $\chi_{\parallel}(T)$ curves of the $Pr_2Fe_{14}BH_x$ compounds. First, $\chi_{\parallel}(T)$ is about 1 order of magnitude smaller for R =Dy, and, second, the small low T peak detected in $\chi_{\parallel}(T)$ for $Nd_2Fe_{14}BH_x$, $Ho_2Fe_{14}BH_x$, and $Dy_2Fe_{14}BH_x$, $x>1$, is clearly smaller and very different in shape than that observed in the $Pr_2Fe_{14}BH_x$, $x<3$, compounds. A similar behavior is also found in the $Tb_2Fe_{14}BH_x$ compounds (see Fig. 5). In the Tb series $\chi_{\parallel}(T)$ is smaller than in the $Dy_2Fe_{14}BH_x$ compounds and no anomalous behavior is found up to T=250 K. The origin of these differences shall be discussed in Sec. V.

B. Magnetic aftereffect measurements

The MAE measurements performed on the $R_2Fe_{14}BH_x$ (R=Gd, Pr, and Dy) are displayed in Figs. 1, 3, and 4. In the $Gd_2Fe_{14}BH_x$ and $Pr_2Fe_{14}BH_x$ series a clear peak appears at the same temperature range at which a drop in $\chi'_{\parallel}(T)$ is observed. The presence of such a peak evidences the existence of mobile defects coupled to the DWs. In the $Dy_2Fe_{14}BH_x$ series the MAE anomaly, although coincident with the drop in $\chi'_{\parallel}(T)$, is very small. The reduction of the MAE signal is a consequence of the small magnetic susceptibility. In fact, the MAE signal of $Dy_2Fe_{14}B$ is, as $\chi'_{\parallel}(T)$, about 1 order of magnitude smaller than that measured in the Pr-based compounds. That is, in this case, the small MAE peak does not mean that there are no mobile defects in the material; it simply reflects that the experimental setup has not enough sensitivity to detect such a tiny magnetic response.

The MAE data displayed in Figs. 1 and 3 have been fitted with expression (1).[21] The best fits are attained by using a pre-exponential factor $\tau_0=10^{-13}$ s and with the average activation energies, $\langle Q \rangle$, displayed in Tables I and II. The values of τ_0, $\langle Q \rangle$, and the shape of the MAE curves indicate that the short-range diffusion of Fe vacancies or H interstitial atoms is the most probable diffusion process that causes the MAE anomaly.[22–24]

V. DISCUSSION

All the studied $R_2Fe_{14}BH_x$ compounds display two kinds of anomalous behaviors, labeled as HT and LT anomalies. The HT anomalies [namely, the drop in $\chi'_{\parallel}(T)$ at T_4 and the steplike rise of $\chi'_{\parallel}(T)$ at T_5 accompanied by a peak in $\chi''_{\parallel}(T)$] can be partly accounted for by the model developed by García *et al.*[5] (in what follows, model 0). In contrast, the behavior at LT is different in each series and cannot be described by this model. Moreover, there are several aspects (see Figs. 1–5) not included in model 0 which have to be taken into account when describing the $\chi_{\parallel}(T)$ behavior:

(i) There is no peak in $\chi''_{\parallel}(T)$ accompanying the drop of $\chi'_{\parallel}(T)$ at T_4 (see Figs. 1–4). In contrast, there is always a peak in $\chi''_{\parallel}(T)$ at T_3 accompanying the LT side of the $\chi'_{\parallel}(T)$ peak.

(ii) The existence of more than one type of mobile defect interacting with the DWs. In the $Gd_2Fe_{14}BH$ compound, the LT anomalies follow the same pattern as the HT ones, which suggests the presence of a second type of interacting defect with lower activation energy. Moreover, in these compounds there are two types of mobile defects, Fe vacancies and H atoms, which can influence the DW mobility.

(iii) The differences between the compounds with R=Gd and Y, which display a relatively high value of $\chi'_{\parallel}(T)$ at low

TABLE I. Activation energies, $\langle Q \rangle$, obtained from the fit of the MAE measurements, and parameters used in the fits performed with Eqs. (6) and (7) and displayed in Figs. 7 and 8. In all cases the value $\tau_0 = 10^{-13}$ s has been used. For $f = 90$ Hz, the high-temperature anomalies have been simulated by using the fitting parameters obtained for $f = 0.9$ Hz.

Compound	$\langle Q \rangle$ (eV) ±0.01	f (Hz)	α_{noneq} (emu/g Oe) ±0.005	Q_B(dis) (eV) ±0.01	$1+\kappa_B$ ±0.1	Q_B(Deb) (eV) ±0.01	α'_{eqB} (emu/g Oe) ±0.005	α''_{eqB} (emu/g Oe) ±0.005	α_{noneqA} (emu/g Oe) ±0.005	Q_A(Dis) (eV) ±0.01	$1+\kappa_A$ ±0.1	Q_A(Deb) (eV) ±0.01	α'_{eqA} (emu/g Oe) ±0.005	α''_{eqA} (emu/g Oe) ±0.005
$Gd_2Fe_{14}BH$	0.59	0.9	0.022	0.08	1.5	0.10	0.063	0.055		0.59	1.4	0.62	0.071	0.063
		90	0.007	0.08	1.5	0.10	0.065	0.041		0.59	1.4	0.62	0.071	0.063
$Gd_2Fe_{14}BH_2$	0.55	0.9		~0.08		~0.10			0.038	0.55	1.4	0.57	0.110	0.095
		90							0.035	0.55	1.4	0.57	0.110	0.095
$Gd_2Fe_{14}BH_3$	0.51	0.9							0.040	0.53	1.2	0.56	0.018	0.021
		90							0.035	0.53	1.2	0.56	0.018	0.021
$Gd_2Fe_{14}BH_4$	0.51	0.9							0.050	0.52	1.1	0.55	0.013	0.016
		90							0.039	0.52	1.1	0.55	0.013	0.016
$Y_2Fe_{14}BH$		90			1.4	0.24	0.026	0.012	0.008	0.59	1.1	0.62	0.017	0.012
$Y_2Fe_{14}BH_{2.5}$		90			1.2	0.19	0.027	0.020	0.004	0.48	1.5	0.53	0.022	0.035
$Y_2Fe_{14}BH_{3.5}$		90			1.2	0.19	0.025	0.021	0.004	0.48	1.4	0.53	0.030	0.044

temperatures, and the compounds with R=Pr, Nd, Dy, Tb, and Ho for which $\chi'_{\parallel}(T)$ is almost zero at low T.

(iv) The differences between the compounds with R=Nd, Ho, and Dy, which display a very small and shapeless low T $\chi'_{\parallel}(T)$ peak, and the compounds with R=Pr, in which the low T $\chi'_{\parallel}(T)$ peak is about 1 order of magnitude greater and displays a clear frequency dependence.

Consequently, it is necessary to improve the initial model. This can be done in three steps. First, it is necessary to refine model 0 for one type of defect. This new model will be referred to as model 1. Second, the model has to be expanded in order to include the influence of two types of defects in $\chi_{\parallel}(T)$. The corresponding model, will be referred to as model 2. Third, it is necessary to consider the influence of the R MCA in order to understand the differences between the R =Gd and Y, R=Pr, and R=Nd, Ho, Dy, and Tb series. The corresponding model for $\chi_{\parallel}(T)$ will be referred to as model 3.

In what follows the focus is on the description of the $\chi_{ac}(T)$, or $\chi_{\parallel}(T)$, anomalous behavior originated by the presence of mobile defects coupled to DWs, $\chi_{md}(T)$. The anomalous component $\chi_{md}(T)$ is superimposed to a background or intrinsic component, $\chi_0(T)$, which is produced both by the reversible rotational processes of the magnetic moments and by the DW motions. The total $\chi_{ac}(T) = \chi_0(T) + \chi_{md}(T)$ will coincide with the measured $\chi_{\parallel}(T)$ whenever the compound exhibits uniaxial anisotropy with the EMD parallel to the c axis of their tetragonal unit cell.

To describe $\chi_{md}(T)$ it is important to bear in mind that the state of the DWs-defects system during the $\chi_{ac}(T)$ measurement depends on the relative values of the relaxation time of the defects, τ_d, the time span for every experimental point, τ_e, and the inverse of exciting frequency, $\omega = 2\pi f$, the so-called experimental time, $\tau_m = 1/\omega$. As for the MAE experiments, it is assumed that the defects relaxation time, τ_d, depends on the temperature following an Arrhenius law, $\tau_d = \tau_0 \exp(Q/k_B T)$, where Q is the mobile defects activation energy and k_B the Boltzman constant.

A. Model 1: $\chi_{md}(T)$ originated by the presence of one type of mobile defect coupled to the DWs

In a standard $\chi_{ac}(T)$ measurement, before starting the data-acquisition process, the sample is cooled from RT to 5 K. At T=5 K the equilibrium distribution of DWs and defect positions are different from that at T=300 K and the defects have to diffuse to the new equilibrium positions. However, at T=5 K the time response of the defects is extremely low, $\tau_d \sim 10^{705}$ s (taking $\tau_0 = 10^{-13}$ s and Q=0.70 eV), and, consequently, the total system has not time enough to achieve the T=5 K equilibrium state when the measurement begins. Provided that τ_d exponentially decreases when the temperature is raised and τ_e is kept constant through the experiment ($\tau_e \sim 180$ s), three regimes of the total system DW defects are possible when increasing T from T=5 K:

(i) Nonequilibrium or metastable regime: temperatures at which $\tau_e \ll \tau_d$ (very low temperatures). In this regime the total DWs-defects system is out of equilibrium and the nonequilibrium response of the DWs, $\chi_{noneq}(T)$, is measured.

(ii) Disaccommodation regime: temperatures at which $\tau_e \sim \tau_d$ (intermediate temperatures). In this temperature range

TABLE II. Activation energies, $\langle Q \rangle$, obtained from the fit of the MAE measurements, and parameters used in the fits performed with Eqs. (6) and (8) and displayed in Figs. 9–12. In all cases the value $\tau_0 = 10^{-13}$ s has been used. For $f = 90$ Hz, the high-temperature anomalies have been simulated by using the fitting parameters obtained for $f = 0.9$ Hz. The values of $1+\kappa_B$ are affected by the low T intrinsic increase of $\chi'_{\parallel}(T)$ (see details in the text).

Compound	$\langle Q \rangle$ (eV) ±0.01	f (Hz)	α_{noneq} (emu/g Oe) ±0.005	Q_B(dis) (eV) ±0.01	$1+\kappa_B$ ±0.1	Q_B(Deb) (eV) ±0.01	α'_{eqB} (emu/g Oe) ±0.005	α''_{eqB} (emu/g Oe) ±0.005	α_{noneqA} (emu/g Oe) ±0.005	Q_A(Dis) (eV) ±0.01	$1+\kappa_A$ ±0.1	Q_A(Deb) (eV) ±0.01	α'_{eqA} (emu/g Oe) ±0.005	α''_{eqA} (emu/g Oe) ±0.005
$Pr_2Fe_{14}B$	0.70	0.9							0.20	0.70				
		90							0.19	0.70				
$Pr_2Fe_{14}BH$	0.62	0.9	0		17.9	0.28	0.21	0.10		0.59				
		90	0		17.9	0.28	0.18	0.10		0.59				
$Pr_2Fe_{14}BH_2$	0.56	0.9	0		19.1	0.25	0.20	0.14		0.54	5.1	0.56	0.21	0.12
		90	0		19.1	0.25	0.16	0.08		0.54	5.1	0.56	0.15	0.12
$Pr_2Fe_{14}BH_3$	0.54	0.9	0		9.6	0.23	0.15	0.10		0.54	2.9	0.54	0.12	0.14
		90	0		9.6	0.23	0.12	0.08		0.54	2.9	0.54	0.10	0.11
$Dy_2Fe_{14}B$		0.9							0.002	0.70				
		90							0.002	0.70				
$Dy_2Fe_{14}BH$		0.9	0								5.9	0.64	0.017	0.009
		90	0											
$Dy_2Fe_{14}BH_2$		0.9	0			0.27	0.004			0.47	5.4	0.59	0.015	0.008
		90	0			0.27	0.003			0.47	5.4	0.59	0.022	0.011
$Dy_2Fe_{14}BH_4$		0.9	0			0.26	0.004			0.44	5.0	0.57	0.017	0.011
		90	0			0.26	0.002			0.44	5.0	0.57	0.016	0.009
$Tb_2Fe_{14}BH$		90	0								5.0	0.64	0.004	0.001
$Tb_2Fe_{14}BH_2$		90	0						0.0001	0.55	6.2	0.59	0.003	0.005
$Tb_2Fe_{14}BH_{2.5}$		90	0								6.1	0.57	0.005	0.001
$Tb_2Fe_{14}BH_3$		90	0								6.7	0.57	0.007	0.003

the time response of the defects becomes comparable to τ_e; hence, the total system can reach the equilibrium state during the measurement of $\chi_{ac}(T)$.

(iii) Equilibrium regime: temperatures at which $\tau_e \gg \tau_d$ (relatively high temperatures). The total system is in thermodynamic equilibrium at each experimental point. Hence, the equilibrium response of the DWs, $\chi_{eq}(T)$, is measured. In this regime the state of the DWs-defects system depends on the relative values of τ_e and τ_m:

(iii.1) When $\tau_d > \tau_m$ (adiabatic regime), the diffusion of the defects is very slow compared to the experimental time. In such a case, during the measurement of one experimental point, the defects are fixed at the equilibrium positions acting as pinning centers of the DWs. This pinning reduces the DW mobility and causes a reduction of $\chi_{eq}(T)$ to the so-called adiabatic susceptibility limit.

(iii.2) When $\tau_d > \tau_m$ (higher T, isothermal regime) the mobile defects can instantly follow the DWs movement during the measurement of one experimental point. Hence, the defects no longer act as pinning centers of the DWs. This unpinning of the DWs produces an increase of $\chi'_{eq}(T)$ to the so-called isothermal susceptibility limit. The increase of $\chi'_{eq}(T)$ from the adiabatic value to the isothermal one takes place when $\tau_d \sim \tau_m$. In this thermal range there is a lag between DW and defect displacements which gives rise to a maximum in $\chi''_{eq}(T)$.

The average susceptibility can be expressed as

$$\chi_{md}(T) = (1 - \phi)\chi_{noneq}(T) + \phi\chi_{eq}(T), \tag{2}$$

where ϕ is the fraction of DWs that for a given time t and at a given temperature T are in thermal equilibrium with the mobile defects. The fraction $\phi = \phi(t,T)$ depends on the temperature, the process that had caused the nonequilibrium state, and the time elapsed since the nonequilibrium situation has been created.

At the beginning of the $\chi_{ac}(T)$ measurement ($t=0$ s and $T=5$ K), the DWs-defect system is in the metastable state, $\phi=0$, and the defects are fixed at some unknown positions. As time elapses, the system evolves toward the thermal equilibrium and ϕ progressively increases up to $\phi=1$. The increase of ϕ will depend on the temperature because the greater the temperature is the faster the diffusion of the defects takes place. This behavior can be modeled by the expression

$$\phi = 1 - \exp(-t/\tau_d). \tag{3}$$

This expression allows (taking $t=\tau_e$) to quantify the state of the total system at each experimental point and describes the entrance of the total system in the adiabatic equilibrium regime when $\tau_d \sim \tau_e$.

When the total system is in the equilibrium regime, $\phi=1$, the anomalous contribution, $\chi_{md}(T)=\chi_{eq}(T)$, has been derived by Wantenaar *et al.*[19] According to their model, when measuring $\chi_{ac}(T)$, the exciting magnetic field exerts an alternating force on the DW, assumed to be pinned in a potential well with an intrinsic damping mechanism; therefore its equation of motion is that of a forced damped oscillator. The restoring force has two contributions: one associated with the intrinsic elastic coupling, that can be considered harmonic, and other corresponding to the attractive potential which describes the interaction between walls and defects that act as pinning centers. Hence, it can be shown that $\chi_{eq}(T)$ is given by the following expressions, which describe the evolution from the adiabatic regime to the isothermal one as a Debye-type relaxation process:[5,19]

$$\chi'_{eq} = \alpha'_{eq}\left[\frac{1 + \omega^2(1+\kappa)\tau_0^2 \exp(2Q/k_BT)}{1 + \omega^2(1+\kappa)^2\tau_0^2 \exp(2Q/k_BT)}\right], \tag{4a}$$

$$\chi''_{eq} = \alpha''_{eq}\left[\frac{\omega\kappa\tau_0 \exp(2Q/k_BT)}{1 + \omega^2(1+\kappa)\tau_0^2 \exp(Q/k_BT)}\right]. \tag{4b}$$

In this expression, α'_{eq} and α''_{eq} are the equilibrium susceptibilities at $T=\infty$ and κ is a phenomenological constant that reflects the interaction potential between DWs and defects.[5,19] The κ constant can be determined from the experimental data, since $\chi'(T\to\infty)=1$ and $\chi'(T\to 0)=1/(1+\kappa)$.

As mentioned above, the anomalous component $\chi_{md}(T)$ is superimposed to a background or intrinsic component, $\chi_0(T)$, which is produced both by the reversible rotational processes of the magnetic moments and by the DWs motion. This contribution should be obtained from the experimental data and the most practical approach is to take $\chi_0(T)$ as the susceptibility of the system in the adiabatic regime. Hence, after subtracting $\chi_0(T)$, $\chi_{md}(T)=\chi_{ac}(T)-\chi_0(T)$ will be zero in the adiabatic equilibrium regime. In such a case, Eq. (4a) is no longer valid to describe $\chi_{md}(T)$, since $\chi'(T\to 0)=1/(1+\kappa)$, and should be renormalized to zero. Hence, if we take $\chi_0(T)$ as the susceptibility in the adiabatic regime $\chi_{eq}(T)$ is then given by the following expressions:

$$\chi'_{eq} = \alpha'_{eq}\left[\frac{1 + \omega^2(1+\kappa)\tau_0^2 \exp(2Q/k_BT)}{1 + \omega^2(1+\kappa)^2\tau_0^2 \exp(2Q/k_BT)} - \frac{1}{1+\kappa}\right]$$
$$= \alpha'_{eq}\Psi(T,\omega), \tag{5a}$$

$$\chi''_{eq} = \alpha''_{eq}\left[\frac{\omega\kappa\tau_0 \exp(2Q/k_BT)}{1 + \omega^2(1+\kappa)\tau_0^2 \exp(Q/k_BT)}\right]. \tag{5b}$$

Moreover, using this expression, $\chi'_{eq}(T)$ can be expressed in terms of $\Psi(T,\omega)$, the fraction of DWs which are in isothermal regime at a given temperature T and for a given excitation frequency ω, which will be useful when describing model 2. In the adiabatic regime, $\Psi(T,\omega)=0$, whereas $\Psi(T,\omega)=1$ in the isothermal state.

Consequently, the final expressions for $\chi_{ac}(T)$ are

$$\chi'_{ac}(T) = \chi_0(T) + (1-\phi)\chi'_{noneq}(T) + \phi\chi'_{eq}(T)$$
$$= \chi_o(T) + e^{(-\tau_e/\tau_d)}\alpha_{noneq} + (1 - e^{(-\tau_e/\tau_d)})\alpha'_{eq}\Psi(T,\omega), \tag{6a}$$

$$\chi''_{ac}(T) = (1-\phi)\chi''_{noneq}(T) + \phi\chi''_{eq}(T). \tag{6b}$$

As in Ref. 5, no anomalous contribution is expected in the metastable regime; hence, in this regime, the thermal dependence of $\chi'_{ac}(T)$ is that of $\chi_0(T)$ and $\chi'_{noneq}(T)$ can be replaced by a positive constant, α_{noneq}. We will discuss below the validity of this assumption.

In the nonequilibrium or metastable regime τ_d is so large that the system has no enough time to achieve its equilibrium state after the time τ_e has elapsed; that is, the defects are fixed and the DWs move due to the ac field. Hence, $\chi'_{ac}(T)$ will be higher than when the system is in equilibrium at that temperature, as we know from MAE experiments (see Sec. IV B). Accordingly, in the metastable regime, an enhanced susceptibility is measured: $\chi'_{ac}(T)=\chi_0(T)+\alpha_{noneq}$, whereas $\chi''_{ac}(T)=0$.

In the adiabatic equilibrium regime, all the DWs are pinned by the defects, $\phi=1$ and $\Psi(T,\omega)=0$. In such a case, there is no anomalous contribution to the total susceptibility; hence, $\chi'_{ac}(T)=\chi_0(T)$ and $\chi''_{ac}(T)=0$. Consequently, in the magnetic disaccommodation regime (that is, in the transition from the metastable regime to the adiabatic one) there would be a gradual reduction of the DWs movement, as they are progressively pinned by the defects, and a drop in $\chi'_{ac}(T)$ is measured. This drop is due to the thermal diffusion of the defects and does not depend on the frequency of the alternating field.

In the isothermal equilibrium regime the pinning potential acting on the defects vanishes; i.e., $\phi=1$ and $\Psi(T,\omega)=1$, and, again, an enhanced susceptibility is measured: $\chi'_{ac}(T)=\chi_0(T)+\alpha'_{eq}$ and $\chi''_{ac}(T)=0$. The transition from the adiabatic to the isothermal regime bears an increase in $\chi'_{ac}(T)$ accompanied by a peak in $\chi''_{ac}(T)$. The temperature at which the transition takes place depends on the frequency of the applied alternating field through the term $\tau_m=1/\omega$. More precisely, the temperature at which the transition takes place increases with the frequency of the applied alternating field.

The response of the DWs in each regime can also be described in terms of the effective potential, Φ_{eff}, acting on the DWs. In the adiabatic regime, $\Phi_{eff}=\Phi_{adi}\neq 0$, whereas in the isothermal one, $\Phi_{eff}=\Phi_{iso}=0$

B. Model 2: $\chi_{md}(T)$ originated by the presence of two types of mobile defect coupled to the DWs

Let us assume that there are two kinds of mobile defects in the system. Each defect is characterized by its activation energy, Q_A and Q_B, $Q_A>Q_B$. For simplicity it is assumed that $\tau_{0A}=\tau_{0B}$ or, equivalently, $\tau_{dA}>\tau_{dB}$. That is, the A defects have a greater relaxation time than the B defects. The potentials acting on the DWs will be called $\Phi_{eff,A}$ and $\Phi_{eff,B}$. In what follows the DWs-A defects subsystem will be referred to as the A subsystem, whereas the DWs-B defects subsystem will be called B subsystem.

As it will be shown below the peculiar behavior observed in $\chi_{ac}(T)$ can only be explained assuming that the potentials $\Phi_{eff,A}$ and $\Phi_{eff,B}$ are not additive. That is, when the mobility of the DWs is reduced by the interaction with one type of defects, the effect of a new pinning center does not produce an additional reduction of the DWs mobility. This behavior can be described by the following expressions, which will be referred to as model 2:

$$\chi'_{ac}(T)=\chi_0(T)+(1-\phi_B)\alpha_{noneq}(T)+(1-\phi_A)\phi_B\chi'_{eqB}(T)+\phi_A\chi'_{eqA}(T) \quad (7a)$$

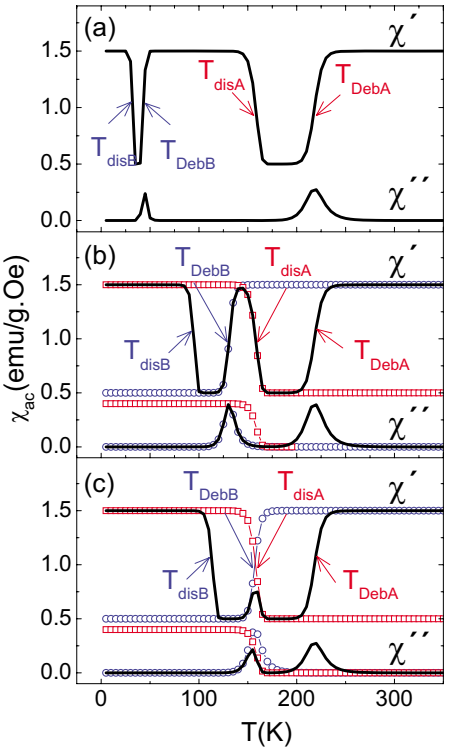

FIG. 6. (Color online) Temperature dependence of χ_{ac} predicted by Eq. (7) in the cases (a) $Q_A=0.5$ eV and $Q_B=0.10$ eV, (b) $Q_A=0.5$ eV and $Q_B=0.30$ eV, and (c) $Q_A=0.5$ eV and $Q_B=0.36$ eV. In cases (b) and (c) there are also displayed the contributions due to the Debye B process (blue open circles) and to the disaccommodation A regime (red open squares).

$$\chi''_{ac}(T)=(1-\phi_A)\phi_B\chi''_{eqB}(T)+\phi_A\chi''_{eqA}(T) \quad (7b)$$

Where the different parameters have the same meaning as in model 1 and $\chi_{eqA}(T)$ and $\chi_{eqB}(T)$ are given by Eqs. (5a) and (5b). The behavior of $\chi_{ac}(T)$ predicted by this expression for different values of Q_A and Q_B is shown in Fig. 6. In all cases, it is taken that $\tau_{0A}=\tau_{0B}=10^{-13}$ s, $1+\kappa_A=1+\kappa_B=5$, $f=0.9$ Hz, and $\alpha_{noneq}=\alpha'_{eqA}=\alpha'_{eqB}=1$.

At $T=5$ K, defects and DWs are in off-equilibrium positions; hence, an enhanced $\chi'_{ac}(T)=\chi_0(T)+\alpha_{noneq}$ is measured. In this regime, $\chi''_{ac}(T)=0$. When the temperature is increased the behavior of $\chi_{ac}(T)$ will depend on the relative values of τ_{dA}, τ_{dB}, τ_e, and τ_m. Since $\tau_{dA}>\tau_{dB}$, the first process to be observed will be the disaccommodation of the B subsystem which takes place at $T=T_{disB}$ (see Fig. 6). At this temperature a drop in $\chi'_{ac}(T)$ takes place when the system enters in the adiabatic regime B. The behavior of $\chi_{ac}(T)$ when the temperature is further increased will depend on the relative values of Q_A and Q_B. Two different cases can be distinguished:

Case (1): Low values of Q_B ($Q_B \ll Q_A$). The disaccommodation of the A subsystem takes place when the B subsystem is in the isothermal state [see Fig. 6(a)]. In such a case, after the drop in $\chi'_{ac}(T)$ at T_{disB}, the transition toward the isothermal regime B at T_{DebB} is observed. When the temperature is further increased, the A subsystem enters in the adiabatic equilibrium regime. Provided that the B system is in the isothermal regime ($\Phi_{eff,B}=\Phi_{iso}=0$), there is no pinning poten-

tial acting on the defects and a new reduction in $\chi'_{ac}(T)$ takes place at T_{disA}. If the temperature is further increased, the transition toward the isothermal regime A at T_{DebA} will be eventually take place. Hence, a plateau in $\chi'_{ac}(T)$ is observed, between T_{DebB} and T_{disA} [see Fig. 6(a)], very similar to that found in $Gd_2Fe_{14}BH$ and $Y_2Fe_{14}BH_{2.5}$ (Figs. 1 and 2).

Case (2): Intermediate or high values of Q_B ($Q_B \leq Q_A$). In this case the disaccommodation of the A subsystem and the transition toward the isothermal state of the B subsystem take place at similar temperature ranges [see Figs. 6(b) and 6(c)].

When the A subsystem enters in the equilibrium regime, at $T=T_{disA}$, only a fraction Ψ_B of the DWs are in isothermal regime with respect to the B defects [where Ψ_B is defined as in Eq. (5)]. This fraction of DWs is not under the action of the B pinning potential. Consequently, their mobility will be drastically reduced at T_{DisA} when they become pinned by the A defects. The difference with case (1) comes from the remaining 1-Ψ_B fraction of DWs, which are pinned by the B defects at $T=T_{disA}$. When the temperature is further increased, the mobility of these DWs should increase as they enter in the isothermal regime (in which the B defects no longer act as pinning centers). However, when the condition $\Phi_{eff,B}=\Phi_{iso}=0$ is attained, these DWs become immediately pinned by the A defects. That is, the transition from the adiabatic to the isothermal regime of this 1-Ψ_B fraction of DWs is interrupted by the presence of the A defects.

In this case a peak in $\chi'_{ac}(T)$ is observed, which is caused by the convolution of the increase in $\chi'_{ac}(T)$ due to the adiabatic-isothermal transition of the B subsystem and the drop in $\chi'_{ac}(T)$ due to disaccommodation regime of the A subsystem [see Figs. 6(b) and 6(c)]. The left side of this peak depends on the frequency of the applied field because it is due to a Debye process; in contrast, the right side is frequency independent because it is due to a disaccommodation process. Moreover, there is a peak in $\chi''_{ac}(T)$ due to the Debye process of the B subsystem.

The heights of the $\chi'_{ac}(T)$ and $\chi''_{ac}(T)$ peaks depend on the relative values of Q_A and Q_B or, more precisely, on the Ψ_B fraction of DWs that are not pinned by the B defects at $T=T_{DebA}$. When $\Psi_B \sim 1$ at $T=T_{disA}$ [relatively low values of Q_B, Fig. 6(b)] a strong peak in $\chi'_{ac}(T)$ is observed. Moreover, as the peak in $\chi''_{ac}(T)$ is not affected by the disaccommodation of the A subsystem, it appears at $T=T_{DebB}$ [see Fig. 6(b)]. On the contrary, when $\Psi_B \sim 0$ at $T=T_{disA}$ [relatively high values of Q_B, Fig. 6(c)] a small peak in $\chi'_{ac}(T)$ is observed. In this case, the out-of-phase component, $\chi''_{ac}(T)$, reflects the convolution of the peak due to Debye process of the B subsystem and the drop due to the disaccommodation regime of the A subsystem [see Fig. 6(c)]. As a consequence, the maximum of the $\chi''_{ac}(T)$ peak is observed at $T<T_{DebB}$ and coincides with the maximum of $\chi'_{ac}(T)$ peak. This kind of $\chi''_{ac}(T)$ behavior cannot be accounted for if one assumes that the pinning potentials are additive. Indeed, in such a case, a peak in $\chi''_{ac}(T)$ due to the B Debye process should be always observed coincident with the inflection point of the left side of the $\chi'_{ac}(T)$ peak.

C. Model 3: Influence of the MCA in $\chi_{ac}(T)$

According to models 1 and 2, at $T=5$ K, $\chi'_{\|}(T)=\chi_0(T)+\alpha_{noneq}$, which should be larger than the susceptibility measured in the adiabatic regime ($T_{disB}<T<T_{DebB}$) (see Fig. 6). However, in $Pr_2Fe_{14}BH_x$ and $Dy_2Fe_{14}BH_x$, it is experimentally found that both $\chi'_{\|}(T)$ and $\chi''_{\|}(T)$ are almost zero at $T=5$ K and increase when the temperature is raised, up to the drop in $\chi'_{\|}(T)$ (see Figs. 3 and 4). These discrepancies indicate that, in these compounds, the nonequilibrium state is more complex than that assumed in the previous models.

The fact that $\chi'_{\|}(T) \sim \chi''_{\|}(T) \sim 0$ at LT indicates that the DWs movement is severely damped at these temperatures. That is, there is an additional influence which hinders the susceptibility from reaching the value corresponding to the nonequilibrium state. There is a relatively simple explanation to this behavior. In the previous models, by analogy with the MAE experiments, it is assumed that the mobility of the defects is greater in the nonequilibrium regime. However, an interaction between defects and DWs exists and their influence can be large when the mobility of the DWs is small.

In magnetically axial systems, the DWs width, δ, is inversely proportional to the square root of the anisotropy effective constant $\delta \sim 1/\sqrt{K_{eff}}$.[3,6,17,25] K_{eff} increases when the temperature is lowered; hence, at low-enough temperatures, the DWs can be so narrow that they can hardly move under the influence of an external magnetic field. In such a case, the influence of the mobile defects (even when they are fixed at off-equilibrium positions) can be strong enough to hinder the small DWs mobility, in such a way that $\chi'_{\|}(T) \sim \chi''_{\|}(T) \sim 0$ at very LT.

When the temperature is raised, the DWs becomes broader, their mobility increases, and they can overcome the pinning of the blocked defects. That is, the system progressively evolves toward a state in which the DWs can freely move following the exciting magnetic field, which explains the $\chi'_{\|}(T)$ increase up to T_{dis}. This argument does not apply for the $Gd_2Fe_{14}BH_x$ and $Y_2Fe_{14}BH_x$ compounds, for which there is no R MCA. For the same reason, in these compounds, both $\chi'_{\|}(T)$ and $\chi''_{\|}(T)$ are not zero at low T.

This hypothesis conciliates the two principal proposed arguments for explaining the non-SRT anomalies in $R_2Fe_{14}B$ and similar compounds.[5,6] However, it should be stressed that it is necessary that both processes coexist to explain the peak in $\chi'_{\|}(T)$. If there are no mobile defects, only an increase in $\chi'_{\|}(T)$ will be observed due to the broadening of the DWs. If there is no influence of the MCA (as in the $Gd_2Fe_{14}BH_x$ or $Y_2Fe_{14}BH_x$ compounds) an enhanced susceptibility will be observed at LT up to T_{dis}.

The simplest expressions to account for the influence of both the MCA and two types of mobile defects in $\chi_{ac}(T)$ are

$$\chi'_{ac}(T) = \chi_0(T) + (1-\phi_A)\phi_B\chi'_{eqB}(T) + \phi_A\chi'_{eqA}(T), \quad (8a)$$

$$\chi''_{ac}(T) = (1-\phi_A)\phi_B\chi''_{eqB}(T) + \phi_A\chi''_{eqA}(T), \quad (8b)$$

where the influence of the MCA has been take into account considering that $\alpha_{noneq}=0$. However, it should be noted that, according to the working hypothesis, the increase of $\chi'_{\|}(T)$ in the 100–175 K range [left side of the $\chi'_{\|}(T)$ peak] is due to the Debye process of the B subsystem and also to the intrinsic increase of the DWs mobility. This additional increase in $\chi'_{\|}(T)$ should result in an enhanced value of $1+\kappa_B$ determined from the experimental data; for instance, in

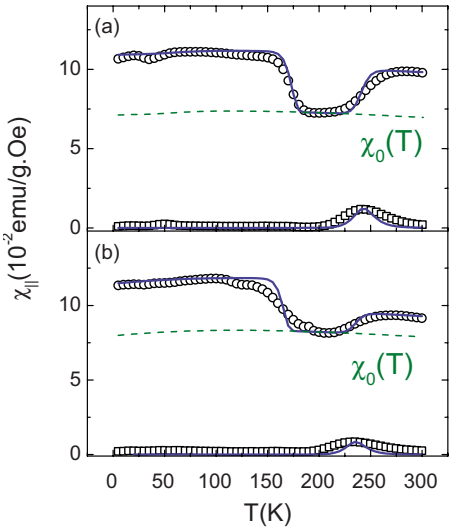

FIG. 7. (Color online) Fitted $\chi_{||}(T)$ curves of (a) $Gd_2Fe_{14}BH_2$ and (b) $Gd_2Fe_{14}BH_3$ measured at $f=0.9$ Hz. In each panel, displayed are the experimental in-phase, $\chi'_{||}(T)$ (open circles), and out-of-phase, $\chi''_{||}(T)$ (open squares) components of $\chi_{||}(T)$, the total fit (blue solid line) of each component and the intrinsic susceptibility $\chi_0(T)$ (green dashed line) used in the fits (see details in the text).

$Pr_2Fe_{14}BH_2$, $f=0.9$ Hz, $1+\kappa_B=17.91$ is obtained, whereas for the same compound and frequency, $1+\kappa_A=5.38$.

D. Fit of the experimental data

1. Compounds with no R MCA: R=Gd and Y

The behavior predicted by model 1 [namely, a drop in $\chi'_{||}(T)$ followed by a steplike rise of $\chi'_{||}(T)$ accompanied by a peak in $\chi''_{||}(T)$] perfectly matches with the anomalies found in $Gd_2Fe_{14}BH_x$ $(x>1)$ [see Fig. 1]. In these compounds $\chi_{ac}(T)=\chi_0(T)+\chi_{md}(T)$ coincides with the measured $\chi_{||}(T)$, since all the compounds are magnetically axial in the measured thermal range. Hence, the experimental curves have been fitted using Eqs. (6a) and (6b). The results are shown in Fig. 7. $\chi_0(T)$ has been taken as $\chi'_{||}(T)$ of the pure $Gd_2Fe_{14}B$, which does not display anomalous behavior, scaled to the values of $\chi'_{||}(T)$ in the adiabatic regime, and the κ constant has been determined from the experimental data taking $\chi'(T\rightarrow\infty)$ and $\chi'(T\rightarrow 0)$ as the values of $\chi'_{||}(T)$ before and after the transition from adiabatic to isothermal regime; for instance, in $Gd_2Fe_{14}BH_2$, $f=0.9$ Hz, $1+\kappa=\chi'_{||}(T=285\ \mathrm{K})/\chi'_{||}(T=195\ \mathrm{K})=1.37$. Small differences between the Q values derived from the fit of the disaccommodation or Debye processes are expected since they are average values and the underlying physical processes are different. Consequently, in the fitting procedure, different Q values for the disaccommodation and Debye processes, labeled as Q(dis) and Q(Deb) were used. The resulting fitting parameters are displayed in Table I. The good quality of the fits demonstrates that in these compounds, the anomalous behavior of $\chi_{||}(T)$ is due to the existence of mobile defects coupled to DWs.

In model 0 it was assumed that a delay exists between the movements of defects and DWs in the disaccommodation regime. Such a delay was modeled as Eq. (4b) taking $\omega=1/\tau_e$.[5] However, this expression predicts a peak in $\chi''_{||}(T)$, accompanying the disaccommodation $\chi'_{||}(T)$ drop, which is not experimentally observed in our samples. Actually, $\chi''_{||}(T)$ cannot be modeled in this way because it is not the same process and, most important, the DWs-defects system is not in thermal equilibrium at these temperatures. According to model 1, $\chi''_{||}(T)$ will be zero in the disaccommodation regime.

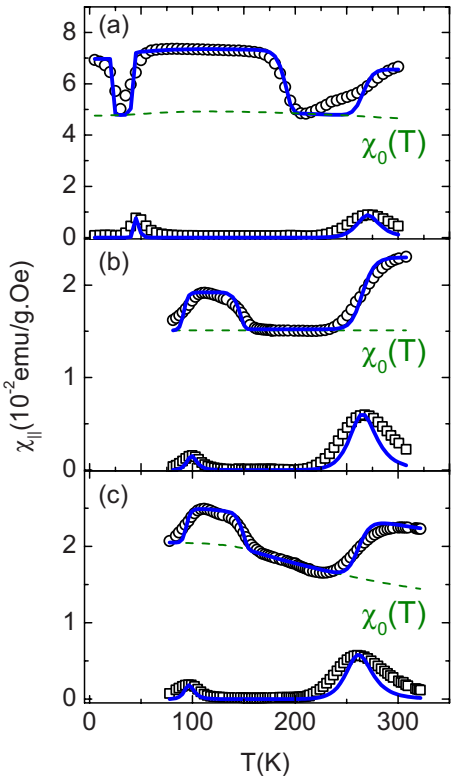

FIG. 8. (Color online) Fitted $\chi_{ac}(T)$ curves of (a) $Gd_2Fe_{14}B$ measured with $f=0.9$ Hz, (b) $Y_2Fe_{14}BH_{2.5}$, and (c) $Y_2Fe_{14}BH_{3.5}$, all measured at $f=90$ Hz. In each panel it is displayed the experimental in-phase, $\chi'_{||}(T)$ (open circles), and out-of-phase, $\chi''_{||}(T)$ (open squares) components of $\chi_{||}(T)$, the total fit (blue solid line) of each component, and the intrinsic susceptibility $\chi_0(T)$ (green dashed line) used in the fits (see details in the text).

It should be noted that the drop in $\chi'_{||}(T)$ due to the disaccommodation process takes place when $\tau_d\sim\tau_e\sim 180$ s, which is approximately the same time window as for the MAE experiments, t_2-$t_1\sim 8-128$ s. The MAE anomaly appears at temperatures at which $\tau_d\sim t_2$-t_1. That is, both techniques measure the same process, the diffusion of the defects, using the same time window, which explains why the MAE anomaly and the drop in $\chi'_{ac}(T)$, or $\chi'_{||}(T)$, take place in the same temperature range.

The behavior of $\chi_{ac}(T)$ in $Gd_2Fe_{14}BH$ and $Y_2Fe_{14}BH_x$ (see Figs. 1 and 2) coincides with that described in case (1) of model 2. Hence, the experimental curves of these compounds have been fitted with Eqs. (7a) and (7b) (see Fig. 8). The κ_A and κ_B constants have been determined from the experimental data as before; for instance, in $Gd_2Fe_{14}BH$, $f=0.9$ Hz, $1+\kappa_B=\chi'_{||}(T=70\ \mathrm{K})/\chi'_{||}(T=30\ \mathrm{K})=146$. For the Y based compounds, $\chi_0(T)$ has been approximated with a linear dependence using the data of $\chi'_{||}(T)$ in the adiabatic regimen, from 140 to 240 K (see Fig. 8). The resulting fitting

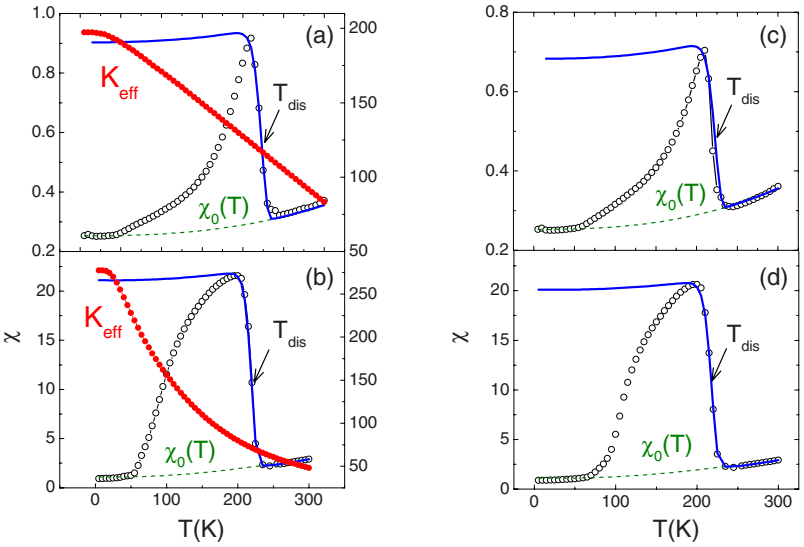

FIG. 9. (Color online) $\chi_{\parallel}(T)$ for (a) $Dy_2Fe_{14}B$, measured at $f=0.9$ Hz, (b) $Pr_2Fe_{14}B$, measured at $f=0.9$ Hz, (c) $Dy_2Fe_{14}B$, measured at $f=90$ Hz, and (d) $Pr_2Fe_{14}B$, measured at $f=90$ Hz. Both the experimental data (open circles) and the theoretical fit predicted by Eq. (6) (blue solid lines) are shown. Dashed green lines correspond to the intrinsic susceptibility, $\chi_0(T)$, used in the fits. The temperature dependence of the effective anisotropy constant is also shown (red solid circles). The nonanomalous contribution $\chi_0(T)$ has been determined by interpolating the behavior of $\chi'_{\parallel}(T)$ at low and high T.

parameters are displayed in Table I. A rough estimation of Q_B for the small disaccommodation process observed in $Gd_2Fe_{14}BH_2$ (see Fig. 2) has also performed and it is also displayed in Table I.

In the $Y_2Fe_{14}BH_x$ compounds, according to the obtained value of Q_B ($\sim$0.20 eV), the corresponding disaccommodation process should take place at $T\sim 60$ K, which is out of the temperature measured range (80–320 K). Hence, only the Debye process associated with the faster, B, defects is visible in $\chi_{\parallel}(T)$.

The good agreement between theory and experiment indicates that (1) in these compounds, the anomalous behavior of $\chi_{\parallel}(T)$ is due to the existence of mobile defects coupled to DWs and (2) there are two kinds of mobile defects coupled to the DWs, which influence is clearly visible in $Gd_2Fe_{14}BH$ and $Y_2Fe_{14}BH_x$. The faster defects cannot be detected with the present MAE measurements because the experimental setup is limited to the temperature range 77–300 K and the MAE anomalies due to the B defects should take place at $T\sim 25$ K in $Gd_2Fe_{14}BH$.

2. *Compounds with R MCA: R*=Pr, Dy, *and* Tb

In the pure $R_2Fe_{14}B$ compounds the most probable diffusing entities are the Fe vacancies; consequently, the $\chi_{\parallel}(T)$ experimental data should be fitted with model 1. However, this model does not account for the $\chi_{\parallel}(T)$ behavior at $T<T_{dis}\sim 250$ K, which is very similar to that observed in the Pr and Dy hydrogenated compounds (see Fig. 9). In contrast, model 1 correctly describes the drop in $\chi'_{\parallel}(T)$ that takes place at $T_{dis}\sim 250$ K (see Fig. 9). The obtained Q values (see Table II) are nearly identical to those obtained from the fit of the MAE curves, confirming that the drop in $\chi'_{\parallel}(T)$ corresponds to the disaccommodation process.

The discrepancies between the fit and the experimental results indicate that the influence of the R MCA should be taken into account. In order to go further into this subject, the temperature dependence of K_{eff} has been determined and compared to $\chi_{\parallel}(T)$ (see Fig. 9). Only the axial anisotropy has been considered since the measurements have been performed onto magnetically oriented samples, that is, $K_{ef}f(T)=K_{1Fe}(T)+K_{1R}(T)+K_{2R}(T)+K_{3R}(T)$, where K_{1Fe} and K_{iR} ($i=1, 2, 3$) are the iron and rare-earth phenomenological anisotropy coefficients, respectively.[26] $K_{1Fe}(T,x)$ has been taken as $K_1(T,x)$ of $Y_2Fe_{14}BH_x$.[27] The K_{iR} constants have been calculated from the CEF parameters, $B_{n0}(x)$,[12] using the linear approach[28] and assuming that the temperature dependence is given by generalized Brillouin functions.[29]

In both Pr and Dy series, K_{eff} is very high and almost constant at LT [when $\chi'_{\parallel}(T)\sim\chi''_{\parallel}(T)\sim 0$] and strongly decreases when increasing T. This decrease coincides with the increase of both $\chi'_{\parallel}(T)$ and $\chi''_{\parallel}(T)$ (Figs. 9–11). Moreover, the decrease of K_{eff} when increasing T is more pronounced in the Pr compounds than in the Dy ones, explaining why $\chi_{\parallel}(T)$ is smaller in the latter compound. This result supports the hypothesis that at very low T, the DWs are very narrow and

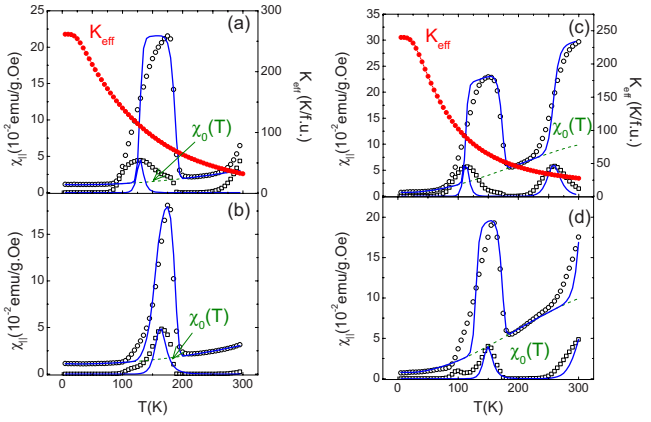

FIG. 10. (Color online) Fitted $\chi_{ac}(T)$ curves of the (a) $Pr_2Fe_{14}BH$ measured at $f=0.9$ Hz, (b) $Pr_2Fe_{14}BH$ measured at $f=90$ Hz, $Pr_2Fe_{14}BH_2$ measured at $f=0.9$ Hz, and $Pr_2Fe_{14}BH_2$ measured at $f=90$ Hz. In each panel, displayed are the experimental in-phase, $\chi'_{\parallel}(T)$ (open circles) and out-of-phase, $\chi''_{\parallel}(T)$ (open squares) components of $\chi_{\parallel}(T)$, the total fit (blue solid line) of each component, and the intrinsic susceptibility $\chi_0(T)$ (green dashed line) used in the fits (see details in the text). The temperature dependence of the effective anisotropy constant is also shown (red solid circles).

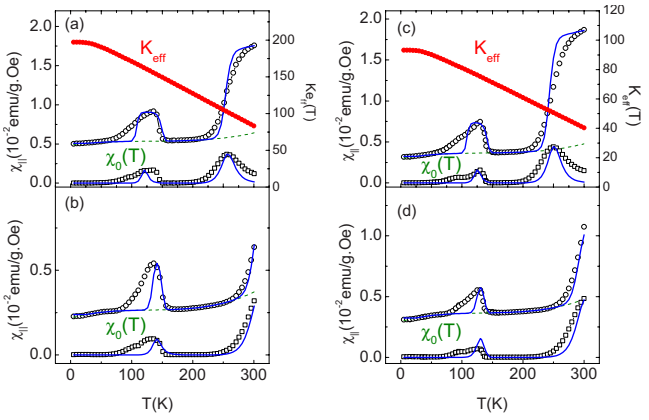

FIG. 11. (Color online) Fitted $\chi_{\parallel}(T)$ curves of the (a) $Dy_2Fe_{14}BH_2$ measured at $f=0.9$ Hz, (b) $Dy_2Fe_{14}BH_2$ measured at $f=90$ Hz, $Dy_2Fe_{14}BH_4$ measured at $f=0.9$ Hz, and $Dy_2Fe_{14}BH_4$ measured at $f=90$ Hz. In each panel, displayed are the experimental in-phase, $\chi'_{\parallel}(T)$ (open circles) and out-of-phase, $\chi''_{\parallel}(T)$ (open squares) components of $\chi_{\parallel}(T)$, the total fit (blue solid line) of each component, and the intrinsic susceptibility $\chi_0(T)$ (green dashed line) used in the fits (see details in the text). The temperature dependence of the effective anisotropy constant is also shown (red solid circles).

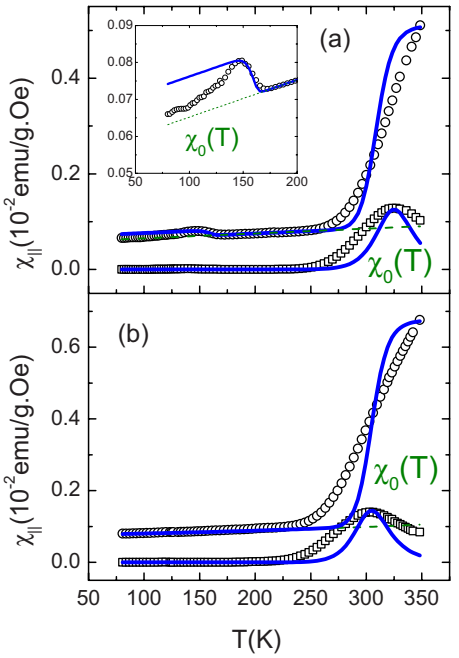

FIG. 12. (Color online) Fitted $\chi_{\parallel}(T)$ curves of the (a) $Tb_2Fe_{14}BH_2$ and (b) $Tb_2Fe_{14}BH_3$ compounds measured at $f=90$ Hz. In each panel, displayed are the experimental in-phase, $\chi'_{\parallel}(T)$ (open circles) and out-of-phase, $\chi''_{\parallel}(T)$ (open squares) components of $\chi_{\parallel}(T)$, the total fit (blue solid line) of each component and the intrinsic susceptibility $\chi_0(T)$ (green dashed line) used in the fits (see details in the text).

posses a very low mobility, which can be damped by the blocked defects, causing that $\chi'_{\parallel}(T) \sim \chi''_{\parallel}(T) \sim 0$ at very LT.

Consequently, the experimental $\chi_{\parallel}(T)$ curves of the $Pr_2Fe_{14}BH_x$, $Dy_2Fe_{14}BH_x$, and $Tb_2Fe_{14}BH_x$ compounds have been fitted by using model 3 [Eqs. (8a) and (8b)]. The fits are shown in Figs. 10–12 and the corresponding fitting parameters are displayed in Table II. The nonanomalous contribution $\chi_0(T)$ has been determined by interpolating the behavior of $\chi'_{\parallel}(T)$ between 5 and 100 K and between 200 and 260 K (see Figs. 10–12). Provided that the convolution of the Debye process of the B subsystem and the disaccommodation process of the A subsystem depend on the measuring frequency, in order to minimize the number of fitting parameters, only data measured with $f=0.9$ Hz have been fitted, whereas data measured with $f=90$ Hz have been simulated using the same Q values.

The $\chi_{\parallel}(T)$ behavior of $Pr_2Fe_{14}BH_x$ ($x<5.5$) at $T>50$ K and $f=0.9$ Hz (see Fig. 3 and 10) coincides with that described in model 2, case (b), whereas the behavior when $f=90$ Hz strongly resembles case (c) of model 2 (see Fig. 6). This coincidence reflects that the Debye process described by Eq. (4) moves to higher temperatures when the alternating frequency is increased, whereas the disaccommodation process does not depend on f. That is, the increase of the alternating frequency for a given Q_B value has the same effect in $\chi_{ac}(T)$ than the increase of Q_B for a fixed value of f.

The end member of the series, the $Pr_2Fe_{14}BH_{5.5}$ compound, displays a $\chi_{\parallel}(T)$ anomalous behavior that cannot be described by any of the previous model: a small $\chi'_{\parallel}(T)$ peak followed by an increase in $\chi'_{\parallel}(T)$ which is almost frequency independent (see Fig. 3). The origin of this peculiar behavior should be searched in the definition of $\chi_{\parallel}(T)$. The anomalous behavior of $\chi_{\parallel}(T)$ can be ascribed to DW displacements and described with Eqs. (8a) and (8b) only when the system is magnetically axial and no anomalous behavior is observed in $\chi_{\perp}(T)$. However, this is not the case for $Pr_2Fe_{14}BH_{5.5}$, which displays a conical magnetic phase in the temperature range of 5–470 K.[12] Hence, the measured $\chi_{\parallel}(T)$ is due to both $\chi_{RR\parallel}(T)$ and to $\chi_{DW}(T)$ and some discrepancies between theory and experiment should be expected.

Regarding the fit of the $Dy_2Fe_{14}BH_x$ compounds, it should be noted that, in this case, it is not possible to obtain accurate values of Q_B(Deb) and Q_A(dis) from the fitting of the experimental data because only a small part of both process is experimentally observed. Indeed, the fit of an incomplete Debye process gives reduced values of Q(Deb), whereas the fit of an incomplete disaccommodation process results in enhanced values of Q(dis). That is, our fitting procedure will result in reduced values of Q_B and enhanced values of Q_A.

Model 3 correctly describes the anomalous behavior of $Dy_2Fe_{14}BH_x$ at $T>175$ K. However, the quality of the fit worsens for $T>175$ K. More specifically, model 3 [Eqs. (8a) and (8b) predicts a frequency dependence on the left side of the $\chi'_{\parallel}(T)$ peak which is not experimentally observed in $Dy_2Fe_{14}BH_x$ (see Fig. 4). Moreover, the Q_A values obtained from the fit of the disaccommodation process of the A subsystem, Q_A(dis) in Table II, are much smaller than the value obtained from the fit of the Debye process of the same subsystem, Q_A(Deb) in Table II. These discrepancies are not due to the fitting procedure, which would lead to enhanced values of Q_A(dis).

Again, the origin of the discrepancies between theory and experiment should be searched in the definition of $\chi_{\parallel}(T)$. In the $Dy_2Fe_{14}BH_x$ compounds, the non-SRT anomalies appear very near to the SRT (see Fig. 4). Hence, when the $\chi_{\parallel}(T)$

peak is observed, the magnetic DWs structure does not consist of 180° domains with their domain walls parallel to the *c* axis and $\chi_{\parallel}(T)$ is due to both $\chi_{RR}(T)$ and to $\chi_{\mathrm{DW}}(T)$. Consequently, in such a case, some discrepancies between theory and experiment should be expected. The same situation is expected for $Nd_2Fe_{14}BH_x$ and $Ho_2Fe_{14}BH_x$ because in both series, a SRT takes place in the same thermal range where the non-SRT anomaly is observed.[2]

This circumstance also explains the strong similarities between the non-SRT anomalies of these compounds and those of the $Pr_2Fe_{14}BH_{5.5}$ (see Fig. 3) which is not magnetically axial in the measured thermal range. The $\chi_{\parallel}(T)$ behavior of $Pr_2Fe_{14}BH_x$, with $x<5.5$, is different because there is no SRT in these compounds. Consequently, the influence of the point defects coupled to DWs can be perfectly described with model 3, as shown before.

In the $Tb_2Fe_{14}BH_x$ compounds, only the HT Debye process is clearly observed in $\chi_{\parallel}(T)$, whereas the LT anomaly is very small ($Tb_2Fe_{14}BH_2$) or inappreciable ($Tb_2Fe_{14}BH_3$). The very small values of $\chi_{\parallel}(T)$ up to 250 K are indicative of a large $K_{\mathrm{eff}}(T)$, which probably hides the LT anomalies. However, since there is no argument to justify the presence of two kinds of mobile defects, the experimental data have been fitted with the simplest hypothesis, that is, assuming that only a type of mobile defect is present in the sample.

Concluding, model 3 correctly describes the anomalous behavior of $\chi_{\parallel}(T)$ only when the system is magnetically axial. When the DW structure differs from that of 180° domains (in the vicinity of a SRT, for example) some deviations from the behavior described by Eqs. (8a) and (8b) should be expected.

E. Diffusing entities and activation energies

The Q and τ_0 values obtained from the fit of the MAE data displayed in Figs. 1 and 3 indicate that the short-range diffusion or Fe vacancies or H interstitial atoms are the most probable diffusion process that causes the MAE anomaly.[22–24] In the $R_2Fe_{14}B$ compounds the short-range diffusion of Fe vacancies is the most reasonable mechanism to explain the MAE anomalies as well as the drop in $\chi'_{\parallel}(T)$, whereas in the hydrogenated compounds both mechanisms, short-range diffusion of Fe vacancies and jump of H atoms between interstitial sites, can influence the DWs mobility.

The existence of Fe vacancies and their mobility depends on the details of the sample preparation,[5] while the H atoms are always present in the hydrogenated samples. Consequently, when only one type of diffusing process is present in hydrogenated samples (as in the $Gd_2Fe_{14}BH_x$, $x>1$ samples) it should be related with the interstitial H atoms. Following this argument, the so-called *A* and *B* defects could be identified as the H atoms and Fe vacancies, respectively. The dependences of Q_A and Q_B on the hydrogen content are shown in Fig. 13. The displayed data correspond to the values obtained from the fit of the Debye processes. In the case of the $Pr_2Fe_{14}BH$ compound (where the Debye process of the *A* subsystem is not observed in the measured temperature range, see Fig. 3) the displayed value of Q_A is Q_A(dis).

The activation energy of the Fe vacancies, Q_B, is almost the same in all the pure compounds and experiences an abrupt decrease when passing from $x=0$ to $x=1$. For $x\geq 1$, the values of Q_B are practically independent on the H concentration. This sudden decrease of Q_B can be understood in terms of the physical changes induced by the hydrogen atoms in the parent compound. In fact, it is known that the $R_2Fe_{14}B$ compounds are converted into powders after the hydrogenation process.[30] This process, known as hydrogen decrepitation, is caused by a large volume expansion of the metal lattice when hydrogen absorbing metallic systems form solid solutions or hydrides.[30] Moreover, the introduction of interstitial atoms in a metallic host modifies the equilibrium distribution of vacancies and their mobility.[31] Indeed, the presence of interstitial hydrogen entails a decrease in the energies of formation and migration of vacancies as well as in their activation energy,[31–33] which explains the observed reduction of Q_B in the hydrogenated samples. The changes in the activation energies have been mainly ascribed to the indirect electronic effect of impurity atoms in the strength of metallic bonds.[33]

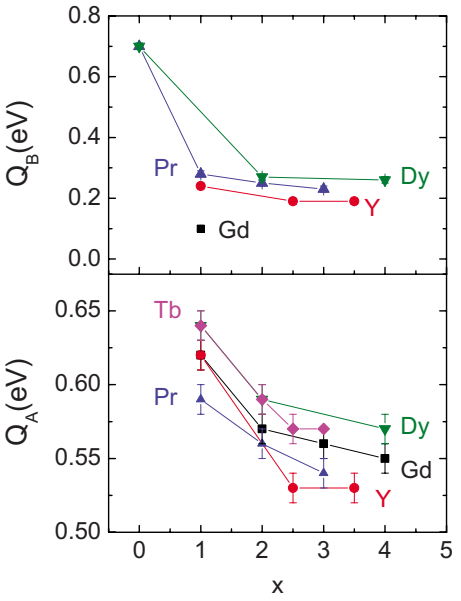

FIG. 13. (Color online). Activation energies of the Fe vacancies (Q_B) and hydrogen atoms (Q_A) obtained from the fit of the $\chi_{\parallel}(T)$ curves of the $R_2Fe_{14}BH_x$, R=Gd (black squares), Y (red circles), Pr (blue up triangles), Dy (green, down-triangles), and Tb (magenta diamonds) series (see details on the text).

The activation energy of the H atoms, Q_A, monotonically decreases when x is increased. The observed dependence of Q_A with x is very similar to that found in $R_2Fe_{14}BH_x$ (R=Ho, Nd) compounds and can be explained with the same simple thermodynamic model.[5] Considering that each interstitial site can be occupied by just one H atom or be empty, a pseudo-Fermi Dirac statistical-mechanics model is applied to the H ensemble. In such a case, the activation energy can be expressed as $Q=E_a-\mu$, where E_a is the average saddle-point energy of the potential wells in which the H atoms are located and μ is the chemical potential, which acts as a pseudo-Fermi level and increases with increasing x.

VI. CONCLUDING REMARKS

The experimental study performed in different $R_2Fe_{14}BH_x$ compounds indicates that the so-called non-SRT anomalies found in the $\chi_{ac}(T)$, or $\chi_{\parallel}(T)$, measurements do not have a unique origin. On the contrary, they can only be correctly described by taking into account the interplay between the influence of mobile defects coupled to the DWs and that of intrinsic properties such as the rare-earth magnetic crystalline anisotropy or the existence of SRTs.

When analyzing the $\chi_{ac}(T)$, or $\chi_{\parallel}(T)$, anomalous behavior four different scenarios are possible, which can be explained with the models described in the present work. In order of complexity:

(1) Compounds with no MCA, no SRTs (such as $Gd_2Fe_{14}BH_x$ and $R_2Fe_{14}BH_x$ with nonmagnetic R), and one type of mobile defects interacting with the DWs. In such a case, the non-SRT anomalies consist in a drop in $\chi'_{\parallel}(T)$ at intermediate temperatures, followed by a steplike increase in $\chi'_{\parallel}(T)$ accompanied by a peak in $\chi''_{\parallel}(T)$. This behavior is that shown in Fig. 1 for $Gd_2Fe_{14}BH$.

(2) Compounds with no MCA, no SRTs, and two types of mobile defects interacting with the DWs. In such a case, the non-SRT anomalies consist in a drop in $\chi'_{\parallel}(T)$ at low temperature, followed by a steplike increase in $\chi'_{\parallel}(T)$ accompanied by a peak in $\chi''_{\parallel}(T)$ at intermediate temperatures. The same behavior is observed at higher temperatures. This behavior is that shown in Figs. 1 and 2 for $Gd_2Fe_{14}BH_x$ ($x>1$) and $Y_2Fe_{14}BH_x$. In cases (1) and (2) the non-SRT anomalies are caused by the interaction between the mobile defects and the DWs.

(3) Compounds with a relatively large MCA at LT, no SRTs, and two types of mobile defects interacting with the DWs. In such a case, both $\chi'_{\parallel}(T)$ and $\chi''_{\parallel}(T)$ are nearly zero at LT and the non-SRT anomalies consist in a large peak in $\chi'_{\parallel}(T)$ and $\chi''_{\parallel}(T)$ at intermediate temperatures, followed by a steplike increase in $\chi'_{\parallel}(T)$ accompanied by a peak in $\chi''_{\parallel}(T)$ at higher temperatures. The left side of the peak in $\chi'_{\parallel}(T)$ depends on the alternating measuring frequency and the maximum of the peak that appears in $\chi''_{\parallel}(T)$ at intermediate temperatures can coincide with the left side of the $\chi'_{\parallel}(T)$ peak or with the maximum of the $\chi'_{\parallel}(T)$ peak, depending on the measuring frequency. This behavior is that shown in Fig. 3 for $Pr_2Fe_{14}BH_x$ ($x<5.5$).

(4) Compounds with a relatively large MCA at LT, SRT, and two types of mobile defects interacting with the DWs. In such a case, both $\chi'_{\parallel}(T)$ and $\chi''_{\parallel}(T)$ are nearly zero at LT and the non-SRT anomalies consist in a small peak in $\chi'_{\parallel}(T)$ and $\chi''_{\parallel}(T)$ at intermediate temperatures, followed by a steplike increase in $\chi'_{\parallel}(T)$ accompanied by a peak in $\chi''_{\parallel}(T)$ at higher temperatures. The left side of the peak in $\chi'_{\parallel}(T)$ depends little on the alternating measuring frequency and the maximum of the χ $\chi''_{\parallel}(T)$ peak coincides with the maximum of the $\chi'_{\parallel}(T)$ peak. This behavior is that shown in Fig. 3 for $Pr_2Fe_{14}BH_{5.5}$ and Fig. 4 for $Dy_2Fe_{14}BH_x$ ($x>1$), and it is also observed in $Nd_2Fe_{14}BH_x$ and $Ho_2Fe_{14}BH_x$.[5] In cases (3) and (4) the non-SRT anomalies result from the interplay between the magnetic DWs structure and the influence of the mobile defects and the MCA on the DWs mobility.

ACKNOWLEDGMENT

Financial aid by the MEC under Contract No. MAT05/1272 is acknowledged.

[1] R. A. Hein, in *Magnetic Susceptibility of Superconductors and Other Spin Systems*, edited by R. A. Hein *et al.* (Plenum, New York, 1991).
[2] J. Bartolomé, M. D. Kuz'min, L. M. García, I. Plaza, D. Fruchart and K. H. J. Buschow, J. Magn. Magn. Mater. **140-144**, 1047 (1995).
[3] D. X. Chen, V. Skumryev, and H. Kronmüller, Phys. Rev. B **46**, 3496 (1992).
[4] M. L. Sartorelli, I. Kleinschroth, and H. Kronmüller, J. Magn. Magn. Mater. **140-144**, 997 (1995).
[5] L. M. García, J. Bartolomé, F. J. Lázaro, C. de Francisco, and J. M. Muñoz, Phys. Rev. B **54**, 15238 (1996).
[6] X. C. Kou, R. Grössinger, G. Hilscher, H. R. Kirchmayr, and F. R. de Boer, Phys. Rev. B **54**, 6421 (1996).
[7] J. Bartolomé, S. Mukherjee, C. Rillo, N. Plugaru, and C. Piquer, J. Alloys Compd. **356-357**, 208 (2003).
[8] F. Canepa, S. Cirafici, M. Napoletano, and R. Masini, Phys. Rev. B **76**, 104402 (2007).
[9] C. Piquer, M. Artigas, and J. Bartolomé, J. Magn. Magn. Mater. **196-197**, 757 (1999).
[10] P. A. Algarabel, J. I. Arnaudas, J. Bartolomé, J. Chaboy, A. Del Moral, J. M. Fernández, M. R. Ibarra, C. Marquina, R. Navarro, and C. Rillo, *Concerted European Action on Magnets* (Elsevier Applied Science, London-New York, 1989), p. 240.
[11] D. Fruchart, L. Pontonnier, F. Vaillant, J. Bartolomé, J. M. Fernández, J. A. Puertólas, C. Rillo, J. R. Regnard, A. Yaouanc, R. Fruchart, and Ph. L'Héritier, IEEE Trans. Magn. **24**, 1641 (1988).
[12] C. Piquer, J. Bartolomé, M. Artigas, and D. Fruchart, Phys. Rev. B **62**, 1004 (2000).
[13] Q. Wang, Z. Zhi-gang, L. Wei, X. C. Sun, Y. C. Chuang, and F. R. de Boer, J. Magn. Magn. Mater. **109**, 59 (1992).
[14] C. de Francisco, J. I. Iñiguez, J. M. Muñoz, and J. Ayala, IEEE Trans. Magn. **23**, 1866 (1987).
[15] K. H. J. Buschow, in *Ferromagnetic Materials*, edited by E. P. Wohlfarth and K. H. J. Buschow (Elsevier, New York, 1988), Vol. 4, Chap. 1.
[16] J. F. Herbst, Rev. Mod. Phys. **63**, 819 (1991).
[17] C. Rillo, J. Chaboy, R. Navarro, J. Bartolomé, D. Fruchart, B. Chenevier, A. Yaouanc, M. Sagawa, and S. Hirosawa, J. Appl. Phys. **64**, 5534 (1988).
[18] M. D. Kuz'min, L. M. García, M. Artigas, and J. Bartolomé, Phys. Rev. B **54**, 4093 (1996).
[19] G. H. T. Wantenaar, G. V. H. Wilson, D. H. Chaplin, and S. J.

Campbell, J. Magn. Magn. Mater. **89**, 13 (1990).
[20] H. J. Blythe, H. Kronmüller, A. Seeger, and F. Walz, Phys. Status Solidi A **181**, 233 (2000).
[21] C. de Francisco, J. I. Iñiguez, and J. M. Muñoz, IEEE Trans. Magn. **25**, 4413 (1989).
[22] H. Kronmüller, in *Hydrogen in Metals I*, edited by G. Alefeld and J. Völkl (Springer-Verlag, Berlin, 1978), Chap. 19.
[23] C. de Francisco, J. M. Muñoz, J. Ayala, and J. I. Iñiguez, Phys. Status Solidi A **108**, 721 (1988).
[24] C. de Francisco, R. Torres, J. M. Muñoz, and J. Rivas, Phys. Status Solidi A **123**, 297 (1991).
[25] S. Chikazumi, *Physics of Magnetism* (Wiley, New York, 1964), Chap. 9, p. 188.
[26] B. P. Hu, K. Y. Wang, Y. Z. Wang, Z. X. Wang, Q. W. Yan, P. L. Zhang, and X. D. Sun, Phys. Rev. B **51**, 2905 (1995).
[27] M. D. Kuz'min, L. M. García, I. Plaza, J. Bartolomé, D. Fruchart, and K. H. J. Buschow, J. Magn. Magn. Mater. **146**, 77 (1995).
[28] C. Rudowicz, J. Phys. C **18**, 1415 (1985).
[29] M. D. Kuz'min, Phys. Rev. B **46**, 8219 (1992)
[30] N. Eliaz, D. Eliezer, and D. L. Olson, Mater. Sci. Eng., A **289**, 41 (2000).
[31] V. A. Goltsov, J. Alloys Compd. **293-295**, 844 (1999).
[32] V. M. Sidorenko, V. V. Fedorov, L. V. Barabash, and V. I. Pokhmurs'kyi, Mater. Sci. **13**, 607 (1978).
[33] Yu. I. Archakov, A. M. Dobrotvorskii, V. I. Pokhmurs'kyi, and V. V. Fedorov, Mater. Sci. **31**, 477 (1995).